CollageMap: Tailoring Generative Fingerprint Map via Obstacle-Aware Adaptation for Site-Survey-Free Indoor Localization

Yeawon You*, JinYi Yoon†, Dayeon Kang‡, Jeewoon Kim§, and HyungJune Lee¶
*Department of Cyber Security, Ewha Womans University, Seoul, South Korea
†Department of Computer Science, Virginia Tech, Blacksburg, VA, USA
‡Manning College of Information & Computer Sciences, University of Massachusetts, Amherst, MA, USA
§Department of Computer Science, University of California, Irvine, CA, USA
¶Department of Computer Science and Engineering, Ewha Womans University, Seoul, South Korea
Email: hyungjune.lee@ewha.ac.kr

***Abstract*—As wireless-equipped devices are widely deployed, fingerprint-based indoor localization becomes popular due to its simple yet precise feature. A key challenge is constructing an accurate map of signals with their corresponding coordinates. However, because the structural layout of each location uniquely affects signal propagation from distinct access points (APs), fingerprint maps cannot be transferred to other locations. This leads to localization failure in unexplored areas. In this paper, we propose *CollageMap*, an obstacle-aware fingerprint map constructor embracing generic signal features and AP-oriented unique features. We tackle the problem of fingerprint construction as a compound of two complementary maps: 1) obstacle-independent *universal map* reflecting *intrinsic* propagation patterns; and 2) obstacle-dependent *adaptation map* representing the *extrinsic* effect of obstacles. We construct a universal model that learns existing fingerprints in various training locations so that it can be generally used at any other place. On top of the universal map, another deep neural network (DNN) learns the real signal deviations between the universal map and the ground-truth map and generates the compensation as the *adaptation map* for obstructed environments. Using real-world received signal strength indicator (RSSI) testbeds across various wireless radios, we have validated *CollageMap* provides outstanding signal pattern estimation even in the presence of obstacles, achieving improvements in localization accuracy of up to 30.36%, 17.95%, and 16.97% using Wi-Fi, ZigBee, and BLE, respectively, via adaptation. *CollageMap* effectively keeps the performance gap of only 0.42%, 17.43 and 7.10% on average, compared to the ground-truth map obtained from the site survey.**

I. Introduction

Indoor localization has become a key technique for enabling location-based applications and services within indoor environments, including real-time navigation, personalized way-finding, and emergency evacuation [1], [2]. With high availability of intelligent devices equipped with Wi-Fi or Bluetooth, they measure a unique set of signal strengths as a *fingerprint* at each reference point and provide opportunities to capture and extract an intrinsic characteristic of wireless signals. Referencing a radio map of these signal fingerprints makes it feasible to locate a user's position instantly, without any additional infrastructure or hardware investments.

As the pre-constructed fingerprint map consequently dominates the robustness of localization [3], some amount of sophisticated signal measurements at a target place is required. However, collecting signal measurements at every single point along with its corresponding coordinates in a region of interest via a *site survey* by humans or robots (with SLAM) be inefficient. To mitigate the labor-intensive and time-consuming processes, some generative model-based approaches have been proposed to supplement limited data points [4], [5]. Beyond the augmentation approaches, it is possible to construct synthetic map, which can be used across various indoor settings [6].

In fingerprint construction, signal strength is attenuated with respect to distance from the transmitting APs. As a result, understanding generic signal propagation behavior affected by travel distance or so is essential for predicting radio signals. This inherent generative map incorporates some generic characteristics of signal propagation, and thus, it can be widely used as a universal map across various contexts.

While distance is a basic factor, it is very difficult to capture the complex nature of radio propagation, which exhibits high variability and uniqueness depending on the presence and density of nearby obstructions, even within the same building or room. For this reason, localization becomes even more challenging in obstructed areas, as the generic map itself is insufficient due to the severe signal interference.

To address this problem, recent works have incorporated distortion patterns caused by obstacles into the concept of ray tracing [7]. However, these approaches typically require highly computationally intensive processing, resulting in critical response latency and necessitating detailed structural information. More closely related to the problem of signal map generation, some works have studied the reconstruction

This work was supported by the Institute of Information & communications Technology Planning and Evaluation (IITP) grant funded by the Korea government (MSIT) (No. RS-2022-00155966, Artificial Intelligence Convergence Innovation Human Resources Development (Ewha Womans University) and No. RS-2021-II212068, Artificial Intelligence Innovation Hub). The corresponding author is HyungJune Lee.

of the fingerprint map from a given original map, focusing on fine-level customized adaptation [8]. In reality, however, obstructions can significantly block and threaten the signal path from a transmitter to a receiver, resulting in alteration. Thus, fingerprint calibration needs to be conducted to adapt to each different surrounding environment.

Now, we raise fundamental questions – *How can we develop a radio fingerprint map that remains applicable to unexplored locations and positions? What is an effective method for accounting for environmental obstructions in order to refine the constructed generic radio map?* It may be necessary to capture *intrinsic* signal fingerprint patterns, and then further adjust environment-dependent *extrinsic* variations caused by surrounding obstruction. By doing so, it may be possible to achieve site-survey-free indoor localization, enriching pervasive indoor localization.

In this paper, we propose *CollageMap*, a novel framework for generating radio fingerprint maps to enable site-survey-free indoor localization. *CollageMap* leverages two neural networks: one for constructing a ***universal map*** that captures general signal propagation patterns and another for creating an ***adaptation map*** that adjusts for environment-specific obstructions. By incorporating environmental information, such as obstacle layouts, *CollageMap* refines fingerprint map, bridging the gap between estimated and actual signal conditions.

To the best of our knowledge, this is the first work that leverages obstacle-awareness to enable site-survey-free indoor localization across different target areas with deep learning models. Our main contributions are summarized as follows:

- We devise a versatile map constructor to calibrate unique distortion caused by surroundings along each different path from APs to a target point on top of a generic radio map significantly advancing indoor localization.
- Based on experiments using real-world RSSI datasets, we validated that *CollageMap* contributes to improving localization performance, by applying *adaptation map* on top of *universal map*, up to 10.52%, and 16.03% at a medium- and to a highly-obstructed place, respectively.
- We validated *CollageMap* using public datasets across various wireless radios, including Wi-Fi, ZigBee, and BLE, as well as datasets with channel state information (CSI). The average localization error distance between the ground-truth map and the *CollageMap*-generated map was 0.01m, 0.38m, 0.12m, and 1.38m, respectively.

In Sec. II, we review related works to provide the context for this study. The overall concept of the proposed scheme is introduced in Sec. III. The detailed procedure for model training and map generation is described in Sec. IV, followed by a comprehensive evaluation in Sec. V. Finally, the paper concludes with a summary in Sec. VI.

II. Related Work

Indoor localization has been a critical research area for decades with early systems paving the way for diverse approaches that estimate the location of a user [9] by leveraging radio signal. The indoor localization research focuses on two distinct types: detailed and fine-scale localization; and pervasive large-scale localization. Fine-scale localization methods are characterized by achieving extremely precise position estimates with sub-centimeter error [10], [11]. This makes them suitable for applications requiring minimal localization error, such as virtual reality systems or navigation systems for individuals with disabilities, where precise tracking of user movement is essential for immersive and extended experiences [12]–[14]. However, infrastructure costs and deployment complexity limit their use in large environments [15], [16].

In contrast, pervasive localization focuses on large-scale, real-world deployments, prioritizing the ease of installation and scalability over pinpoint accuracy [17]. This approach is well-suited for environments such as malls, airports, or parking lots, where a few meters of error is acceptable. Fingerprint-based localization, a crucial tool for pervasive localization, involves an offline phase in which a radio map is constructed by collecting signal measurements at various reference points within the target place. This is followed by an online phase, where the user's location is estimated by comparing current signal measurement with the pre-constructed map. This method enables smartphone-based localization without the need for specialized hardware [18], [19].

Despite its wide adoption, fingerprint-based localization faces notable challenges. The most significant challenge is the burden of the offline phase, which requires extensive manual site surveys to construct fingerprint maps by collecting signal data at multiple reference points This process is time-consuming, labor-intensive, and susceptible to environmental changes such as the movement of furniture, the presence of people, and device heterogeneity, all of which degrade the accuracy of the pre-constructed maps [20]–[22].

Recent efforts to mitigate these challenges include techniques such as data augmentation and generative map construction, where synthetic signal measurements are used to reduce the need for exhaustive on-site data collection [23]–[26]. Some studies have explored the use of ray tracing and obstacle-aware models to learn features for predicting signal propagation in complex environments [27], [28], but these approaches often come with significant computational costs and are site-specific, limiting their applicability to particular locations. Additionally, other research focuses on mitigating errors in fingerprint maps caused by environmental changes, though these methods typically require an initial map to be collected before they can be applied [29].

Our proposed system, *CollageMap*, builds upon these existing approaches by addressing the key challenges of site-survey-free fingerprinting through a novel obstacle-aware fingerprint map generation framework. Unlike traditional methods that rely on extensive on-site surveys or purely synthetic maps, *CollageMap* constructs an initial universal map that captures generic signal propagation patterns and combines it with an adaptation map to account for environmental obstructions. This approach enables efficient and scalable indoor localization without the burdens of site surveys, making it highly suitable for pervasive localization scenarios.

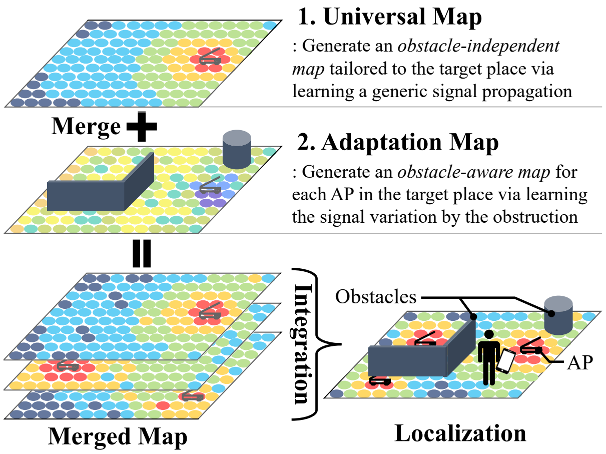

Fig. 1: Map generation process of *CollageMap* for an obstacle-aware fingerprint map generation

III. System Architecture

This paper addresses the challenge of generating realistic radio fingerprint maps for indoor localization. Our objective is to create a scenario in which on-site signal collection, commonly known as a site survey, is unnecessary. Building an accurate map without a site survey is difficult due to environmental variability and the presence of noise. To address this, we propose to infer a realistic radio map that captures both intrinsic signal propagation features, which are generally applicable for any place, and extrinsic features, which are influenced by environmental obstructions. This enables extensive and efficient on-the-fly radio map generation for indoor localization eliminating the need for a site survey.

We propose *CollageMap*, a novel obstacle-aware fingerprint map generation framework that integrates two complementary maps: 1) an obstacle-independent *universal map* and 2) an obstacle-dependent *adaptation map* as shown in Fig. 1. To develop this framework, we recognize that a fingerprint map consists of signal measurements from multiple APs. Since the signal from each AP follows a generic propagation pattern, decomposing the fingerprint map into AP-specific maps is more efficient, improving generalization. Additionally, this approach helps capture environment-specific features, as obstacles affect signal fading patterns differently based on their relative position to each AP. Extracting these detailed features enhances fidelity of the maps for specific target places. Although movable objects like desks and chairs may introduce dynamic effects, potentially confusing the model, we focus on permanent structures, such as walls and pillars, as the primary sources of obstruction to mitigate this issue.

The *universal map* focuses on presenting a generalized map that is free from factors that introduce noise. Next, the *adaptation map* is generated to serve as a bridge between the signal propagation pattern represented by the *universal map*, and that of a specific obstructed environment. The *adaptation map* generation model learns by considering the density of surrounding obstructions and the distance from each AP to various points. For each AP, the model predicts the expected fingerprint gap between the *universal map* and the ground-truth fingerprints of the obstructed environment. The merged map is formed by merging the *adaptation map* with the *universal map* through element-wise fingerprint vector addition. A set of merged maps is then constructed for the existing APs, integrated in a final fingerprint map for the target location. The overall procedure of our obstacle-aware fingerprint map generation framework consists of three steps.

1) **Segmentation**: Decompose the entire fingerprint map into a set of AP-oriented maps by separating the signal strength vector into individual signal strength values for each AP in the training environments
2) **Map Generation**:
   a) **Universal Map**: Predict a *universal map* that captures general signal propagation characteristics for each AP
   b) **Adaptation Map**: Generate a complementary fingerprint gap map relative to the *universal map* by accounting for the level of obstacles
   c) **Merged Map**: Combine the *universal map* with the *adaptation map* to create a merged map that reflects the new AP distributions within the target environment
3) **Integration**: Construct the final fingerprint map by compiling multiple merged maps for a set of APs

IV. Obstacle-aware map generation

We present *CollageMap*, an obstacle-aware fingerprint generation framework designed for new target areas without requiring on-site signal data collection. The framework first extracts features to construct a *universal map* using the first model, based on various fingerprint measurements. It then calculates the discrepancy between the *universal map* and real fingerprint maps from training areas with different obstruction levels. A second model is trained to compensate for these discrepancies, adapting the generated map to specific environments, as illustrated in Fig. 2.

To generate a realistic *universal map* that accurately reflects the major factor affecting signal propagation patterns, distance, we employ an auxiliary classifier generative adversarial network (AC-GAN) model [30] as the first model. Specifically, AC-GAN is designed to generate fingerprints corresponding to the distance between an AP and a given point. We choose AC-GAN because it not only captures the inherent variability in signal propagation without excessive smoothing, but also facilitates stable training while incorporating auxiliary information for more diverse and accurate outputs. This *universal map* then serves as a scalable, generic baseline fingerprint map, applicable to any location.

The *adaptation map* is generated using a deep neural network (DNN) model, chosen for its simplicity, ease of training, and ability to effectively capture the relationship between input and output variables. The DNN learns the correlation between obstruction levels, derived from the building's structural information, and the errors observed in the *universal*

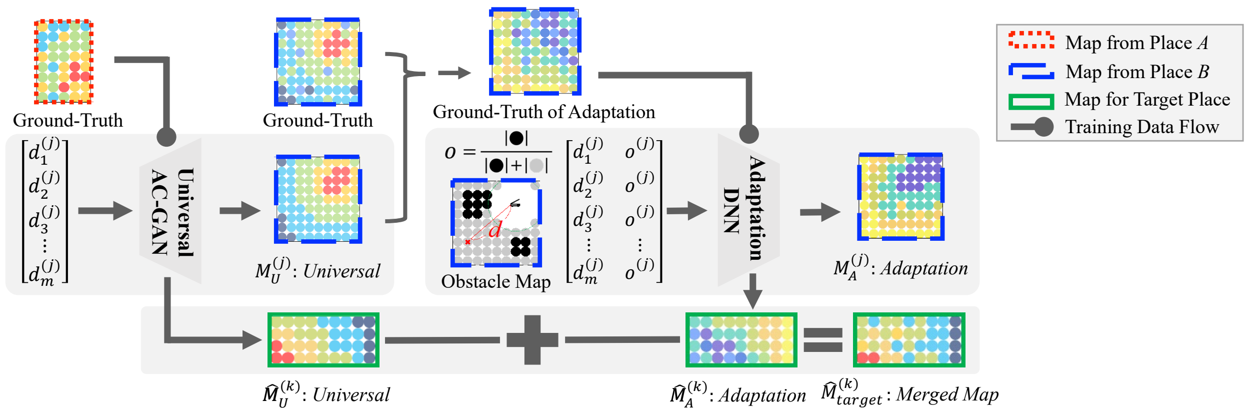

Fig. 2: Our *CollageMap* architecture with AC-GAN for the *universal map* generation and DNN for the *adaptation map* generation. Places A and B are used to train AC-GAN and DNN, respectively, and Place C is the target place

map. By referencing these errors, the second model adjusts the *universal map* to account for the effects of environment-specific obstacles, thereby enhancing its accuracy. Once both the *universal* and *adaptation maps* are generated, an AP-oriented merged map is created by merging them. To form the complete fingerprint map, the individual AP-wise maps for each existing AP in the test area are integrated, making the system ready for localization in a new test environment.

A. Fingerprint Map Segmentation

In the first step of training, we segment the single fingerprint map of signal measurement into AP-wise fingerprint maps, effectively dividing them into n_{AP} maps, each corresponding to a single AP. The fingerprint map, M, is a set of data collected from a real-world testbed, where each data point consists of an signal measure vector and its corresponding coordinates, defined as:

$$M = \{(C_1, S_1), (C_2, S_2), \cdots, (C_{n_{data}}, S_{n_{data}})\}, \quad (1)$$

where $C_i = \{x_i, y_i\}$ represents the coordinates, and $S_i = \{s_i^{(1)}, s_i^{(2)}, \cdots, s_i^{(n_{AP})}\}$ is the signal measure vector for n_{AP} APs. The number of points in the radio map M is n_{data}.

Since signal strength decays relative to the distance from each AP, we segment the signal measurement vectors into n_{AP} individual signal measure values along with their coordinates. Using the known AP coordinates, we replace these coordinates with their relative distances to the AP. The decomposed map $M^{(j)}$ for the j-th AP is given by:

$$M^{(j)} = \{(d_1^{(j)}, s_1^{(j)}), (d_2^{(j)}, s_2^{(j)}), \cdots, (d_{n_{data}}^{(j)}, s_{n_{data}}^{(j)})\}, \quad (2)$$

where $d_i^{(j)}$ is the distance from coordinate C_i to the j-th AP.

B. Map Generation

The merged map for each AP at the target location is generated through three steps: creating two complementary maps and then merging them. Each step will be explained in detail in the following subsections.

1) Universal Map Generation: The generation of the *universal map* is intended to capture the general signal propagation patterns, which are primarily influenced by the distance from an AP. To achieve this, the AC-GAN is trained to learn and predict the *universal map* based on the distance from the transmitting AP. This model generates signal measurement value, fingerprint, that serve as a baseline representation of the signal measurement distribution.

We design an AC-GAN model, referred to as the *universal AC-GAN* in Fig. 2, that takes the relative distance $d_i^{(j)}$ as input and outputs the corresponding signal measure vector $s_i^{(j)}$ for each data point i and AP j. The training data consists of:

$$M_U = \{(d_1^{(1)}, s_1^{(1)}), (d_1^{(2)}, s_1^{(2)}), \cdots, (d_{n_{data}}^{(n_{AP})}, s_{n_{data}}^{(n_{AP})})\}. \quad (3)$$

Upon completing training, the *universal AC-GAN* generates signal measurement value $\hat{s}i^{(j)}$ for the given distance inputs $d_i^{(j)}$. This process is repeated $ndata \times n_{AP}$ times to construct the *universal map*.

2) Adaptation Map Generation: To improve the *universal map*, we integrate an *adaptation map* designed to minimize the error between the *universal map* and the ground-truth, accounting for obstructions in the training environment.

The DNN model, referred to as the *adaptation DNN* in Fig. 2, captures the impact of obstacles on signal attenuation. Initially, a *universal map* for the training area is generated. Subsequently, a ground-truth *adaptation map* is computed by measuring the discrepancy between the two:

$$\begin{gathered} \delta_i^{(j)} = s_i^{(j)} - \hat{s}_i^{(j)} \\ \text{for } i \in \{1, 2, \cdots, n_{data}\} \text{ and } j \in \{1, 2, \cdots, n_{AP}\}, \end{gathered} \quad (4)$$

where $\delta_i^{(j)}$ is the error between the ground-truth value $s_i^{(j)}$ and the predicted value $\hat{s}_i^{(j)}$.

To train the *adaptation DNN* to associate the discrepancies, $\delta_i^{(j)}$, with obstructions, we first generate a binary map of obstacles at the grid level using building or room layout information, as illustrated in Fig. 2, where obstacles are represented by black-colored grid points, with non-obstructed areas in grey. The level of obstruction for each AP is then calculated as the ratio of black points to grey points:

$$o^{(j)} = \frac{\text{\# of obstructed points}}{\text{\# of total points}} \tag{5}$$

where $o^{(j)}$ is the level of obstruction from j-th AP in the place.

The level of obstruction is calculated by excluding points that are too close to the AP. This decision is guided by the intuition that obstacles near an AP have a relatively smaller impact on signal propagation. According to typical signal propagation models, such as the log-distance model [31], signal strength decreases rapidly over short distances, with distance being the dominant factor. As the distance increases, the rate of signal degradation stabilizes, making the signal more susceptible to interference from obstacles. Consequently, obstacles located close to the AP contribute less significantly to signal attenuation compared to those further away.

By focusing on regions farther from the AP, where obstacles have a more pronounced effect on signal strength, we obtain an obstacle ratio that more accurately captures the true impact of the environment on signal propagation. For instance, in the obstacle map shown in Fig. 2, the ratio is calculated using only points outside a defined radius, ensuring a realistic reflection of how obstructions affect the signal. Thus, the *adaptation DNN* is trained using the dataset as follows:

$$M_A^{(j)} = \{(d_1^{(j)}, o^{(j)}, \delta_1^{(j)}), \cdots, (d_{n_{data}}^{(j)}, o^{(j)}, \delta_{n_{data}}^{(j)})\}. \tag{6}$$

After training, during the inference phase, the *adaptation DNN* uses the distance from the AP, $d_1^{(j)}$, and the level of obstruction, $o^{(j)}$, to generate the *adaptation map*. This process is repeated across all areas to adjust the *universal map*, refining signal predictions based on environmental obstructions.

3) Merging for Merged Map Generation: By combining the *universal map* and the *adaptation map* for a given target environment, we generate an AP-specific merged map:

$$\hat{M}_{target}^{(j)} = \{(C_1, \hat{s}_1^{(j)} + \hat{\delta}_1^{(j)}), \cdots, (C_{n_{data}}, \hat{s}_{n_{data}}^{(j)} + \hat{\delta}_{n_{data}}^{(j)})\} \tag{7}$$

where the predicted signal values from the *universal map* are $\hat{s}_i^{(j)}$, and the adjustments from the *adaptation map* are $\hat{\delta}_i^{(j)}$.

C. Integration for Whole Fingerprint Map Construction

During the offline phase, *CollageMap* generates a fingerprint map from scratch for localization, using AP locations and obstruction levels, eliminating the need for a site survey.

To create a complete fingerprint map, we combine the merged map of each AP into a single map with signal measurement vectors for all APs:

$$\hat{M}_{target}^{(j)} = \{(C_1, \hat{S}_1), (C_2, \hat{S}_2), \cdots, (C_{n_{data}}, \hat{S}_{n_{data}})\}, \tag{8}$$

where $\hat{S}_i = \{\hat{s}_i^{(1)} + \hat{\delta}_i^{(1)}, \hat{s}_i^{(2)} + \hat{\delta}_i^{(2)}, \cdots, \hat{s}_i^{(n_{AP})} + \hat{\delta}_i^{(n_{AP})}\}$. The fingerprint for each coordinate is finally generated as a vector of signal measures.

Without collecting any on-site signal data, the generated fingerprint map is used for fingerprint-based localization with existing offline algorithms, such as the NN algorithm, where the position of the user, C_i, is estimated by identifying the fingerprint $\hat{S}_i$ that best matches the user's signal measurements.

The overall algorithm of *CollageMap* for fingerprint map generation is summarized in Algorithm 1.

Algorithm 1 Obstacle-aware fingerprint map generation for site-survey-free localization in *CollageMap*

Input: O: skeleton map of the obstacle distribution, AP: the location of APs, S_{user}: signal strength vector collected in the target place
Output: $\hat{C}_{target}$: estimated position of the user

// Offline phase to generate the radio map
M_U = *universal_map_generation* (AP);
M_A = *adaptation_map_generation* (O, AP);
for $\hat{s}_i^{(j)} \in M_U$ where $j \in AP$ **do**
  for $\hat{p}_i^{(j)} \in M_A$ with all data point i in the target place **do**
    $\hat{M}_{target}^{(j)}$ = $\hat{M}_{target}^{(j)} \cup \{(C_i, \hat{s}_i^{(j)} + \hat{\delta}_i^{(j)}\}$;
  end for
end for
$\hat{M}_{target}$ = *integration*($\hat{M}_{target}^{(1)}$, $\hat{M}_{target}^{(2)}$, $\cdots$, $\hat{M}_{target}^{(n_{AP})}$);

// Online phase to find the user's position
$\hat{C}_{target}$ = *localization* ($\hat{M}_{target}$, S_{user});

Function *universal_map*(AP)
  for $j \in AP$ **do**
    $\hat{M}_U^{(j)}$ = *AC-GAN.generate*(j);
  endfor
end Function

Function *adaptation_map*(O, AP)
  for $j \in AP$ **do**
    $o^{(j)}$ = *calculate_level_of_obstruction*(O, j);
    $\hat{M}_A^j$ = *DNN.predict*($o^{(j)}$);
  endfor
end Function

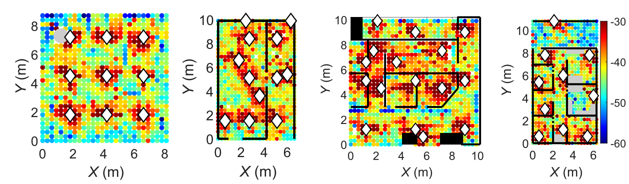

(a) Free space (b) Low-Obs. (c) Medium-Obs. (d) High-Obs.

Fig. 3: The heatmaps of collected maximum RSSI for each differently obstructed place in real-world, where the APs are marked as a white diamond, and the permanent obstacles and temporary obstacles are colored in black and gray, respectively. Furniture is not regarded as obstacles, and the closed doors denoted as a dotted line are considered obstacles

V. Evaluation

We validated *CollageMap* in three different datasets from 10 in-building rooms with different wireless interfaces of Wi-Fi, Zigbee, and BLE.

Model Configurations. We used TensorFlow 2.3.0 and Python 3.8 to implement *CollageMap* with two learning models. For *universal map* generation, we employed an AC-GAN model with a discriminator and generator, each featuring a hidden layer of 128 neurons and ReLU activation. Random noise z, sampled from a uniform distribution in the range of 0.0 to 1.0 with a dimension of 100, was used. RMSProp was the optimizer, set with a learning rate of 0.001 for 500 epochs.

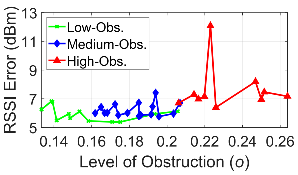

Fig. 4: RSSI error with respect to the level of obstructions for each AP at three different places

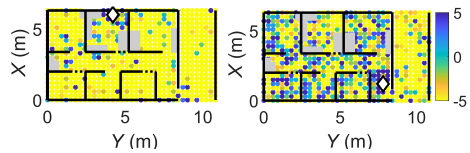

(a) AP #4 (b) AP #8

Fig. 5: RSSI error heatmaps of the *universal map* compared to the ground-truth map for different APs in *High-Obs.*

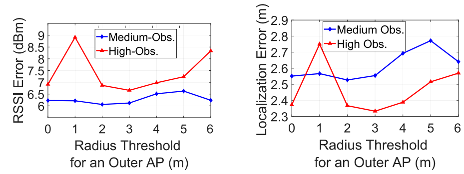

(a) RSSI error (b) Localization error

Fig. 6: RSSI and localization errors of *CollageMap* with respect to different obstacle threshold distances

For *adaptation map* generation, we utilized a DNN model with three hidden layers (128, 64, and 32 neurons) and ReLU activation. We applied the Adam optimizer with a learning rate of 0.001 and a batch size of 32 for 500 epochs.

The *universal map* generation model used mean squared error (MSE) as its loss function, while the *adaptation map* generation model also employed MSE. To prevent overfitting, we implemented early stopping for the DNN with a patience of 50 epochs. All models were trained and tested on an Intel i7-10700F CPU running at 2.90 GHz. Training the AC-GAN required 2 minutes and 44.38 seconds, while training the DNN took 4 minutes and 15.82 seconds. A map for a single AP covering an area of $6.3 \times 10.8m^2$ with 756 grid points could be generated in 0.43 seconds.

Datasets. We evaluated *CollageMap* using three datasets across diverse environments and wireless technologies.

(i) ***Our Wi-Fi RSSI dataset*** consisting of four places: Our testbed environment included homogeneous Wi-Fi APs of EFM-Networks ipTIME N104Q-i with a single antenna of 150mbps on the 2.4 GHz band. We used an LG G Pad 3 10.1 Android tablet to measure the RSSI. We used a grid size of $0.3m$, as shown in Fig. 3. It was collected in four different indoor environments, varying the obstacle density: 1) *Free Space* environment had minimal obstructions, with an average obstacle ratio of 0.051, and 831 data points were gathered over an area of $8.1 \times 8.7m^2$; 2) *Low-Obs.* environment, with an average obstacle ratio of 0.159, comprised 764 data points across $6.6 \times 9.9m^2$; 3) *Medium-Obs.* environment, where the obstacle ratio increased to 0.183, with 1,067 data points over $9.9 \times 9.9m^2$; and 4) *High-Obs.* is the most obstructed environment with an average obstacle ratio of 0.232 and 756 data points collected over an area of $6.3 \times 10.8m^2$.

(ii) ***Public Wi-Fi, Zigbee, and BLE dataset*** [32] consisting of three places: We used this dataset to evaluate the adaptability of *CollageMap* to different wireless technologies, including Wi-Fi, BLE, and ZigBee. This dataset covered three environments (Places A, B, and C), where RSSI measurements from APs were recorded along with corresponding locations.

(iii) ***Public CSI dataset*** [33] consisting of three places: This dataset, collected in three indoor spaces (*Mini Lab*, *Meeting Room*, and *Lab*), provided CSI measurements from three antennas across 30 subcarriers for each AP, offering a more detailed signal profile.

Baselines. To benchmark the performance of *CollageMap*, we compared it against several baseline algorithms, spanning both traditional and machine learning-based approaches: 1) *Log-Distance Model*; and 2) *ITU Propagation Model*. Both models require manual parameter tuning based on the target environment. These traditional models can generate generic radio maps, but typically struggle in environments with high obstruction due to their reliance on pre-configured parameters.

On the machine learning side, we evaluated *CollageMap* against 3) *SelectiveGAN*: to augment fingerprint data using a GAN to reduce the total amount of offline data collection needed. Furthermore, we implemented several online phase algorithms such as 4) *ROCRSSI*: to use minimal ground-truth fingerprint data for localization without constructing full map; 5) *RADAR*: to use a nearest-neighbor-based method for localization; 6) *WiDeep*: to denoise user RSSI measurements using pre-trained autoencoders for better accuracy; and 7) *wkNN*: to use a weighted k-nearest neighbor algorithm. Among these, *CollageMap* showed its availability, particularly in environments with more obstruction, due to obstacle-awareness.

A. Observations from Real-world Datasets

We first evaluated the impact of obstacles on fingerprinting by assessing the RSSI error of the *universal map* compared to the ground-truth map for each AP at three differently obstructed places. We used the mean absolute error (MAE) as the performance metric of RSSI errors, mainly caused by the surroundings of APs. As shown in Fig. 4, the presence of more obstacles leads to greater difficulty in accurately generating a radio map. This inaccuracy in the radio map impedes precise localization, making it necessary to adapt the *universal map*, especially in areas with significant obstructions.

Impact of obstruction on RSSI. Taking a closer look at the actual RSSI error for each AP in a *High-Obs.* environment (see Fig. 5), the gap between predicted and ground-truth RSSI varies based on both the predicted point and the position of AP. As shown in Fig. 5(a), AP #4, deployed inside a room with door closed, requires more aggressive adaptation of the *universal map*. In contrast, AP #8, located in a relatively open space, requires fewer adjustments, as shown in Fig. 5(b). The RSSI error distribution suggests that APs encountering higher levels of obstacles are more prone to error, even within the same area, underscoring the need for individual AP-level adaptation.

Impact of RSSI error on localization. We also explored RSSI and localization errors by varying the measurement area to assess the impact of obstructions. Near the AP, RSSI values

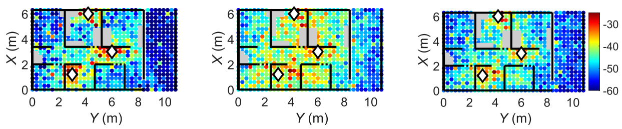

(a) Ground-Truth map of maximum RSSI (b) *Universal map* of maximum RSSI (c) *CollageMap* of maximum RSSI

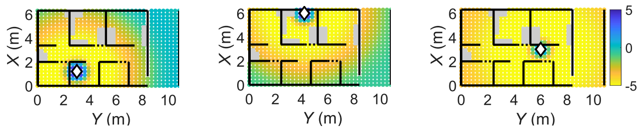

(d) *Adaptation map* of AP #1 (e) *Adaptation map* of AP #4 (f) *Adaptation map* of AP #6

Fig. 7: Heatmaps of generated maps using AP #1, #4, and #6 in *High-Obs.*, where *CollageMap* in (c) patches *adaptation maps* in (d)-(f) onto the collection *universal maps* in (b)

are inherently strong and distinguishable; however, obstacles tend to influence signal strength at greater distances. For example, in *High-Obs.*, a $5dBm$ RSSI error at $1m$ from the AP might result in a sub-0.5m localization error, while the same RSSI error at a $5m$ distance could yield over a $1m$ localization error. We investigated the obstruction levels beyond the circled region using various radius threshold values (see Fig. 6). A threshold of 3.0m proved effective in mitigating both RSSI and localization errors, as RSSI values tend to remain strong within a $3m$ radius of the AP. Subsequently, we applied a 3.0m radius threshold to the outer AP in the experiments.

B. Effect of Fine-Tuning

We primarily used data from the *Free Space* environment to train a *universal map* generation model. Simultaneously, we used data from two different obstructed locations, distinct from the target environment, to form the training set for the *adaptation map* generation model. Notably, at least two distinct locations are essential for training both the universal and adaptation models. All APs were used for training, but to ensure realism, we used only a subset of APs for localization in the target environment. In the *Free Space*, *Low-Obs.*, and *High-Obs.* environments, three APs were employed, proportionate to the RoI size, while *Medium-Obs.* used five APs. During the online phase, we employed the weighted k-nearest neighbor (wkNN) algorithm [34] unless otherwise stated. The evaluation involved five trials conducted over a 0.3m grid, chosen for simplicity and faster inference, though finer granularity could offer improved performance. The results were averaged across all possible combinations of deployable access points to minimize the bias in AP distribution.

Effect of *adaptation map* on RSSI error correction. In Fig. 7, we display several maps: the *universal map* (Fig. 7(b)), *adaptation maps* for individual APs (Figs. 7(d), 7(e), and 7(f)), and the consolidated *CollageMap* (Fig. 7(c)), alongside the ground-truth map (Fig. 7(a)). Notably, the *adaptation maps* are tailored to each AP's characteristics. By applying these adaptations to the *universal* map, we generate the *CollageMap*.

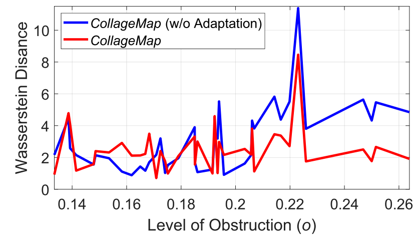

Fig. 8: Wasserstein distance between *CollageMap* and the ground-truth map

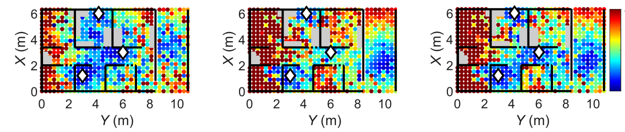

(a) Ground-Truth map (b) *Universal maps* (c) *Merged map*

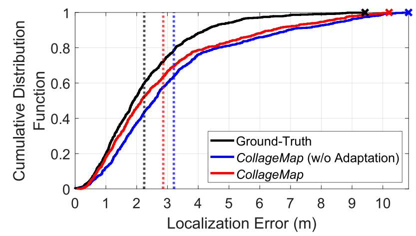

(d) CDF for localization error, where vertical lines indicate the average localization error

Fig. 9: Heatmaps and cumulative distribution of the localization error using AP set of #1, #4, and #6 in *High-Obs.*

Evidently, the *universal map* shows a tendency toward over-prediction, but our point-wise adaptation effectively mitigates the discrepancy with the ground-truth map.

To measure how *adaptation maps* reduce the discrepancy, we computed the Wasserstein distance [35] between AP-wise maps with and without adaptation compared to the ground-truth. As shown in Fig. 8, the *adaptation map* significantly reduces the Wasserstein distance in most scenarios. In particular, in high-obstruction scenarios, our *adaptation map* minimizes the error effectively.

Localization performance of the Fine-tuned map. We analyzed how RSSI error correction improves localization performance, as shown in Fig. 9. The heatmaps, displayed in Figs. 9(a), 9(b), and 9(c), respectively represent the localization error of ground-truth map, the stacked *universal maps*, and the merged map. These show that the final merged map closely aligns with the ground-truth map. In Fig. 9(d), we present both the average localization error and the error distribution. On average, our *CollageMap* reduced the performance gap with the ground-truth by 9.53%. Furthermore, there was a notable increase in the proportion of points with errors below $4m$. Although it remains challenging to completely address the long-tail problem, the *adaptation map* mitigated it.

C. Performance Analysis and Ablation Study

We present a comprehensive evaluation of *CollageMap* through a series of experiments examining various components of the system.

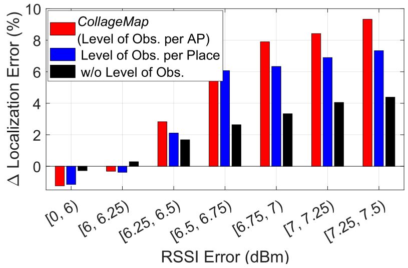

Fig. 10: Performance with different adaptation granularity levels to calculate obstruction effects

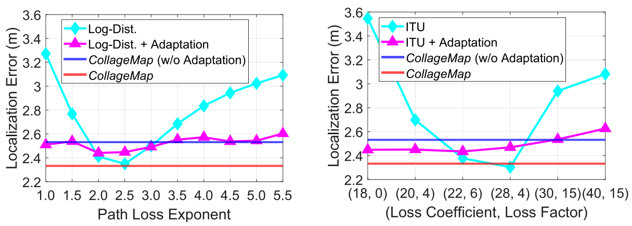

(a) *Universal map* from the log-distance model

(b) *Universal map* from the ITU propagation model

Fig. 11: Effect of adaptation on *universal maps* generated by traditional propagation models

Adaptation Granularity Comparison. In this experiment, we explore the optimal granularity for adaptation in *CollageMap* by comparing two approaches: using only distance information and incorporating place-wise obstacle information to learn adaptation required to compensate for errors in the *universal map*. The first approach ("w/o Obs. Ratio" in Fig. 10) uses only distance information, while the second ("Obs. Ratio per Place") includes obstacle information at the place level, where APs in the same area share an obstruction level, *o*.

To evaluate the effectiveness of *adaptation maps*, we grouped data points into seven categories based on the RSSI error of the *universal map* relative to the ground-truth in *Medium-Obs.* and *High-Obs.* environments. As shown in Fig. 10, AP-wise *adaptation maps*, which utilize obstacle information and differ for each AP, outperform the other two in both RSSI prediction and localization accuracy. Furthermore, the performance gap widens in cases requiring more adaptation, indicating that per-AP adaptation effectively identifies and corrects the primary cause of error. These findings suggest that finer-grained, per-AP adaptation is more effective, especially in environments with unevenly distributed obstacles.

Comparison with Traditional Propagation Models. This experiment compares *CollageMap* with traditional non-machine learning radio propagation models, such as the log-distance [36] and ITU [37] models in *High-Obs.* environment. These models require manual inspection of the target site to set their parameters. As shown by the cyan-colored lines in Fig. 11, the choice of parameters significantly impacts the localization performance using generated map, placing a heavy burden on selecting the 'right' parameters—often unrealistic without on-site RSSI data for verification. When using these models as the *universal map*, training an *adaptation map* generation model can mitigate the difficulty of parameter selection by learning to compensate for errors caused by incorrect parameter choices, as indicated by the stable magenta-colored line in Fig. 11. The best performance, however, is observed with the final merged map itself, depicted by the red line in Fig. 11. This highlights ability of *CollageMap* to generate a map that fits the target environment without the need for human inspection.

Comparison with Alternative Mapping Approaches. We compared *CollageMap* with other mapping methods, including the ITU model, *ROCRSSI* [38], which uses a minimal amount of ground-truth fingerprints instead of a full map, and *SelectiveGAN* [4], which augments fingerprints using a GAN. As shown in Fig. 12, *CollageMap* outperformed all these approaches on average, particularly in the *High-Obs.* environment. Notably, *ROCRSSI* and *SelectiveGAN* rely on a certain amount of on-site radio signal data, whereas *CollageMap* achieves its performance by learning general features of fingerprint maps from other environments and then applying them. This ability to generalize and adapt without requiring specific on-site radio signal data is remarkable.

Comparison of Algorithms for Online Phase. In this experiment, we evaluated *CollageMap* with various localization algorithms during the online phase: RADAR [39], WiDeep [40], and wkNN [34]. As shown in Fig. 13, RADAR underperformed compared to the others. This is because it identifies only the single closest matching point from the generated radio map, which works best when the measured RSSI and the recorded values are assumed to be identical at the same location. In contrast, WiDeep uses pre-trained autoencoder models to denoise the received user RSSI, attempting to find the most similar point on the radio map in the absence of noise. This approach outperformed RADAR. Since the average localization error introduced by the online algorithm is less than a meter, *CollageMap* can achieve precise localization when combined with various online phase algorithms. The choice of an online phase algorithm can further be tailored based on additional factors, such as computational cost and environmental dynamics.

Impact of Varying AP Density. This experiment assesses the scalability of *CollageMap* by testing localization performance with varing numbers of deployed APs in the *High-Obs.* environment. We varied the number of APs from 1 to 5, calculating the average localization error for all possible combinations of AP distribution sets. As shown in Fig. 14, *CollageMap* consistently demonstrated low localization errors, even with fewer deployed APs, maintaining close proximity to the performance achieved using ground-truth data. This highlights the algorithm's scalability and robustness across different AP densities.

D. Various Wireless Radios and Signal Measures

To demonstrate the effectiveness of *CollageMap* across various wireless radios and signal measurements, we conducted tests using publicly available data.

Various Wireless Radio. We examine how generalizable *CollageMap* is according to various wireless radios such as

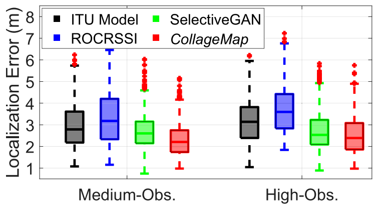

Fig. 12: Comparison with other map generation methods during the offline phase in two different test environments

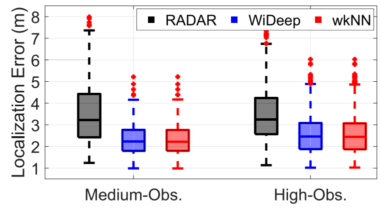

Fig. 13: Performance comparison of different localization algorithms during the online phase

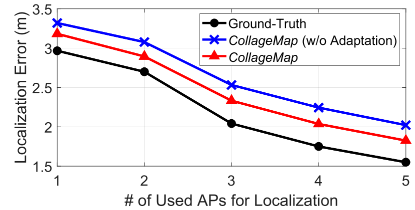

Fig. 14: Localization accuracy with respect to the number of deployed APs in the *High-Obs.* environment

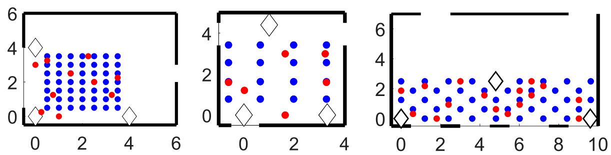

(a) Place A (b) Place B (c) Place C

Fig. 15: Floor plans of three different places, with lines indicating the layout of obstacles, AP locations denoted as diamonds, and the placement of evenly and randomly distributed points represented by blue and red dots, respectively.

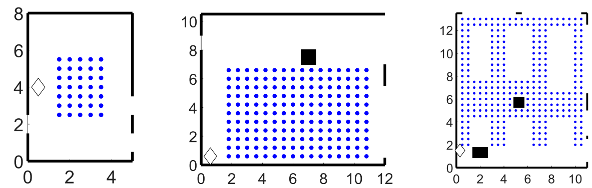

(a) *Mini Lab* (b) *Meeting Room* (c) *Lab*

Fig. 16: Floor plans of three rooms where CSI data were collected. The black lines indicate hard walls, the black squares represent pillars, the blue points show reference points, and the white diamonds mark AP locations.

TABLE I: Localization errors for different radio

Fingerprint Map	**BLE**	**ZigBee**	**Wi-Fi**
Ground-Truth	1.69 m	2.18 m	2.33 m
CollageMap (w/o *Adaptation map*)	2.18 m	3.12 m	3.36 m
CollageMap (w/ Adaptation map*)*	1.81 m	2.56 m	2.34 m
Performance Impact	(- 0.37m)	(- 0.56m)	(- 1.02m)

Bluetooth Low Energy (BLE), ZigBee, and Wi-Fi. As illustrated in Fig. 15, we evaluated on three places, from a public dataset of RSSI measurements [32]. We trained our model using the total dataset of both evenly- and randomly-distributed data. Fingerprints were generated for the evenly-distributed points, and performance evaluation was conducted using the randomly-distributed points. To implement *CollageMap* for testing in a target environment, we used two other locations for training: one for the *universal map* generative model and the other for the *adaptation map* generative model. We assessed performance using all possible combinations of these three locations and calculated the average localization error.

As shown in Table I, our fine-tuned *CollageMap* consistently achieved localization accuracy close to that of ground-truth maps, with error margins of only $0.01m$, $0.38m$, and $0.12m$ for Wi-Fi, ZigBee, and BLE, respectively. Notably, *CollageMap* further reduced localization errors by $0.37m$, $0.56m$, and $1.02m$, respectively, demonstrating its effective compensation through the *adaptation map*. This result highlights *CollageMap*'s adaptability to different radio systems.

CSI Dataset. *CollageMap* can also be applied to generate fingerprint maps using CSI, which has recently been used to achieve better localization accuracy [41]. To verify this, we used a public CSI dataset [33] collected in three different rooms, as illustrated in Fig. 16. For this experiment, we used the data collected in the *Mini Lab* to train the *universal map* generation model, while data from the *Meeting Room* was used to train the *adaptation map* generative model. The training data

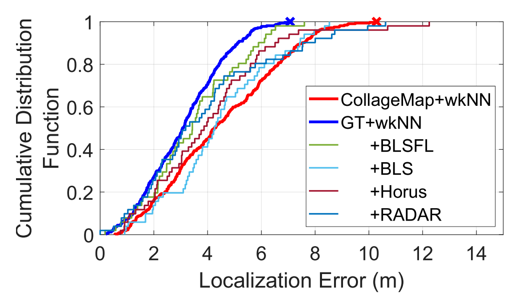

Fig. 17: The cumulative distribution of the localization error in the Lab, where the thick red line represents the results using *CollageMap*, while the thin lines indicate various localization methods that use the on-site collected ground-truth map.

was arranged based on the number of pillars, which served as obstructions in each location. Finally, we generated the CSI fingerprint map for the *Lab* and used the data collected there as input from the user during the online phase. The main difference between the RSSI and CSI data is that the CSI data contains signal measurements from three antennas with 30 sub-carriers each. Therefore, the original framework was modified to accommodate the corresponding input and output sizes, while other settings remained unchanged. Fig. 17 illustrates the performance of *CollageMap* (thick red line) in comparison with the results of online algorithms, including the broad learning system (BLS and BLSFL) [33], RADAR [39], and Horus [42], where all other algorithms have used the ground-truth map. Our result with *CollageMap* and wkNN performs similarly to those using the ground-truth map. This demonstrates that *CollageMap* can effectively generate CSI fingerprint maps with high generalizability.

E. Discussion and Limitation

In Sec. V-A, we verified the generation of an obstacle-aware *adaptation map* using the proposed obstruction level o, demonstrating its effectiveness in producing precise fingerprint maps and enabling accurate localization, as shown in Sec. V-B. Additionally, *CollageMap* outperformed existing baselines across various settings (Sec. V-C) and proved applicable to multiple signal measurement types (Sec. V-D).

CollageMap, which utilizes two deep learning models to generate signal maps, offers distinct advantages over both traditional methods and recent alternatives. Unlike traditional approaches that require parameter tuning for each specific location, our method simplifies map generation by training a model capable of accounting for varying levels of obstructions. This eliminates the need for manual adjustments and improves the overall efficiency of the process. Additionally, compared to GAN-based map generation methods, our adaptation model streamlines the process by allowing the generated maps to be adjusted dynamically for different environments, thereby removing the need for engineers to train separate models for each target location. Furthermore, the demonstrated compatibility of our approach with existing on-line phase algorithms underscores its practical applicability and robustness.

The limited dataset used in this study leaves opportunities for *CollageMap* to be tested in additional environments, such as those featuring different signal frequencies (e.g., 5GHz Wi-Fi) or larger, multi-floor spaces with more complex structures. While *CollageMap* prioritizes simplicity and integrates obstacle awareness to enhance accuracy, future work could explore incorporating additional factors to create even more precise maps. Examples include detailed information about obstructions, such as the presence of furniture, the texture of obstacles, dependencies between APs or devise heterogeneity. Investigating methods to effectively incorporate such data into the model represents an intriguing direction for future research.

Future work could also explore extending the capabilities of *CollageMap* to generate 3D maps or maps for outdoor environments, which would offer additional utility. For 3D mapping, incorporating detailed locations of APs and data points could enhance localization accuracy and enable integrated mapping for multi-story buildings. For outdoor environments, while GNSS generally provides reliable localization, there are situations where their performance is suboptimal – for instance, in urban areas densely packed with tall buildings that obstruct satellite signals or in regions covered by sunshades. In such scenarios, a pervasive fingerprint-based localization system could serve as an effective alternative. *CollageMap* has the potential to address these challenges if adapted to account for additional environmental factors such as weather conditions.

To relax the assumption that building structure information is required, various indoor mapping methods can be utilized. A straight-forward approach is to reference emergency evacuation plans, which are commonly posted on each floor in many buildings and provide realistic and simplified structural layouts. In cases where such plans are unavailable, alternative low-cost indoor mapping methods can be employed. Examples include the use of kinetic sensors and ZED stereo cameras [43], or even advanced techniques like mmWave radar [44], which has shown a promise in extreme conditions such as smoky environments.

Although *CollageMap* still has room for improvement, its contribution is significant in that it enables indoor localization without the need for extensive signal strength dataset collection and shows that the quality of the generated maps can be enhanced by referencing meta-information of target place such as floor plans. In addition to its strength in enabling instant localization even in large-scale environments, *CollageMap* has a potential to evolve into a crowd-aware or obstacle-material-aware map generator by learning how various factors contribute to map errors, positioning it as a promising pillar for more accurate and pervasive localization.

VI. Conclusion

We introduced *CollageMap*, a novel framework for constructing obstacle-aware radio maps enabling fingerprint-based indoor localization without on-site signal data collection. Our method employs two complementary learning models, AC-GAN and DNN, to generate two types of maps: a *universal map* that captures general signal propagation patterns and an *adaptation map* that accounts for signal variations due to obstructions. This dual-model method bridges the gap between the generic *universal map* and the real-world radio map.

CollageMap focuses on constructing radio maps in obstructed environments by incorporating the impact of obstacles on signal strength, factoring them as AP-wise. By applying the *adaptation map* to *the universal map*, our framework improves localization accuracy by up to 16.03% in highly obstructed settings. Furthermore, *CollageMap* enables site-survey-free localization with only a 14.6% average performance gap compared to manually collected ground-truth fingerprint maps. Importantly, it is radio-agnostic, capable of generating fingerprint maps for various technologies such as BLE, Zigbee, and Wi-Fi, and works with any signal metrics, verified with RSSI and CSI.

References

[1] S.-J. Yoo and S.-H. Choi, "Indoor ar navigation and emergency evacuation system based on machine learning and iot technologies," *IEEE Internet of Things Journal*, vol. 9, no. 21, pp. 20853–20868, 2022.

[2] R. Ayyalasomayajula, A. Arun, C. Wu, S. Sharma, A. R. Sethi, D. Vasisht, and D. Bharadia, "Deep learning based wireless localization for indoor navigation," in *Proceedings of the 26th Annual International Conference on Mobile Computing and Networking*, pp. 1–14, 2020.

[3] B. Huang, R. Yang, B. Jia, W. Li, and G. Mao, "A theoretical analysis on sampling size in wifi fingerprint-based localization," *IEEE Transactions on Vehicular Technology*, vol. 70, no. 4, pp. 3599–3608, 2021.

[4] W. Njima, M. Chafii, A. Chorti, R. M. Shubair, and H. V. Poor, "Indoor localization using data augmentation via selective generative adversarial networks," *IEEE Access*, vol. 9, pp. 98337–98347, 2021.

[5] H. Zou, C.-L. Chen, M. Li, J. Yang, Y. Zhou, L. Xie, and C. J. Spanos, "Adversarial learning-enabled automatic wifi indoor radio map construction and adaptation with mobile robot," *IEEE Internet of Things Journal*, vol. 7, no. 8, pp. 6946–6954, 2020.

[6] G. B. Tarekegn, R.-T. Juang, H.-P. Lin, L.-C. Tai, Y. Y. Munaye, and M. A. Bitew, "Srcloc: Synthetic radio map construction method for fingerprinting outdoor localization in hybrid networks," *IEEE Sensors Journal*, vol. 22, no. 15, pp. 15574–15583, 2022.

[7] V.-H. Nguyen, V. Corlay, N. Gresset, and C. Ciochina, "Probabilistic ray-tracing aided positioning at mmwave frequencies," in *2023 13th International Conference on Indoor Positioning and Indoor Navigation (IPIN)*, pp. 1–6, IEEE, 2023.

[8] P. Wilk, J. Karciarz, and J. Swiatek, "Indoor radio map maintenance by automatic annotation of crowdsourced wi-fi fingerprints," in *2015 International Conference on Indoor Positioning and Indoor Navigation (IPIN)*, pp. 1–8, IEEE, 2015.

[9] R. Want, A. Hopper, V. Falcao, and J. Gibbons, "The active badge location system," *ACM Transactions on Information Systems (TOIS)*, vol. 10, no. 1, pp. 91–102, 1992.

[10] K. M. Bae, H. Moon, and S. M. Kim, "Supersight: Sub-cm nlos localization for mmwave backscatter," in *Proceedings of the 22nd Annual International Conference on Mobile Systems, Applications and Services*, pp. 278–291, 2024.

[11] G. Zhang, G. Chi, Y. Zhang, X. Ding, and Z. Yang, "Push the limit of millimeter-wave radar localization," *ACM Trans. Sen. Netw.*, vol. 19, apr 2023.

[12] M. Rietzler, M. Deubzer, T. Dreja, and E. Rukzio, "Telewalk: Towards free and endless walking in room-scale virtual reality," in *Proceedings of the 2020 CHI Conference on Human Factors in Computing Systems*, pp. 1–9, 2020.

[13] M. Murata, D. Ahmetovic, D. Sato, H. Takagi, K. M. Kitani, and C. Asakawa, "Smartphone-based indoor localization for blind navigation across building complexes," in *2018 IEEE International Conference on Pervasive Computing and Communications (PerCom)*, pp. 1–10, IEEE, 2018.

[14] S. A. Cheraghi, V. Namboodiri, and L. Walker, "Guidebeacon: Beacon-based indoor wayfinding for the blind, visually impaired, and disoriented," in *2017 IEEE International Conference on Pervasive Computing and Communications (PerCom)*, pp. 121–130, IEEE, 2017.

[15] T. Margiani, S. Cortesi, M. Keller, C. Vogt, T. Polonelli, and M. Magno, "Angle of arrival and centimeter distance estimation on a smart uwb sensor node," *IEEE Transactions on Instrumentation and Measurement*, vol. 72, pp. 1–10, 2023.

[16] Y.-T. Chan, W.-Y. Tsui, H.-C. So, and P. chung Ching, "Time-of-arrival based localization under nlos conditions," *IEEE Transactions on Vehicular Technology*, vol. 55, no. 1, pp. 17–24, 2006.

[17] J. Ni, F. Zhang, J. Xiong, Q. Huang, Z. Chang, J. Ma, B. Xie, P. Wang, G. Bian, X. Li, *et al.*, "Experience: Pushing indoor localization from laboratory to the wild," in *Proceedings of the 28th Annual International Conference on Mobile Computing And Networking*, pp. 147–157, 2022.

[18] B. Shin, T. Kim, H. Kyung, C. Yu, D. Shin, and T. Lee, "Vehicle tracking system in underground parking lots using smartphone," *IEEE Transactions on Intelligent Transportation Systems*, 2024.

[19] Y. Hu, F. Qian, Z. Yin, Z. Li, Z. Ji, Y. Han, Q. Xu, and W. Jiang, "Experience: Practical indoor localization for malls," in *Proceedings of the 28th Annual International Conference on Mobile Computing And Networking*, pp. 82–93, 2022.

[20] L. Zhang, S. Wu, T. Zhang, and Q. Zhang, "Learning to locate: Adaptive fingerprint-based localization with few-shot relation learning in dynamic indoor environments," *IEEE Transactions on Wireless Communications*, vol. 22, no. 8, pp. 5253–5264, 2023.

[21] H. Zhang, J. Hu, H. Zhang, B. Di, K. Bian, Z. Han, and L. Song, "Metaradar: Indoor localization by reconfigurable metamaterials," *IEEE Transactions on Mobile Computing*, vol. 21, no. 8, pp. 2895–2908, 2022.

[22] A. Poulose and D. S. Han, "Performance analysis of fingerprint matching algorithms for indoor localization," in *2020 International Conference on Artificial Intelligence in Information and Communication (ICAIIC)*, pp. 661–665, 2020.

[23] S. A. Junoh and J.-Y. Pyun, "Enhancing indoor localization with semi-crowdsourced fingerprinting and gan-based data augmentation," *IEEE Internet of Things Journal*, 2023.

[24] S. Sarkar, A. Baset, H. Singh, P. Smith, N. Patwari, S. Kasera, K. Derr, and S. Ramirez, "Llocus: Learning-based localization using crowd-sourcing," in *Proceedings of the Twenty-First International Symposium on Theory, Algorithmic Foundations, and Protocol Design for Mobile Networks and Mobile Computing*, pp. 201–210, 2020.

[25] Y. Wei and R. Zheng, "Handling device heterogeneity in wi-fi based indoor positioning systems," in *IEEE INFOCOM 2020-IEEE Conference on Computer Communications Workshops (INFOCOM WKSHPS)*, pp. 556–561, IEEE, 2020.

[26] J. Yoon, Y. You, D. Kang, J. Kim, and H. Lee, "Gan-loc: Empowering indoor localization for unknown areas via generative fingerprint map," in *2024 21st Annual IEEE International Conference on Sensing, Communication, and Networking (SECON)*, pp. 282–290, IEEE, 2024.

[27] Q. Liu, S. Xu, J. W. Lee, C. Yuen, and S. G. Razul, "A ray-tracing based fingerprinting method for passive localization in urban nlos environment," in *ICASSP 2024-2024 IEEE International Conference on Acoustics, Speech and Signal Processing (ICASSP)*, pp. 8631–8635, IEEE, 2024.

[28] S. Fan, Y. Wu, C. Han, and X. Wang, "A structured bidirectional lstm deep learning method for 3d terahertz indoor localization," in *IEEE INFOCOM 2020-IEEE Conference on Computer Communications*, pp. 2381–2390, IEEE, 2020.

[29] D. Li, J. Xu, Z. Yang, and C. Tang, "Train once, locate anytime for anyone: Adversarial learning-based wireless localization," *ACM Transactions on Sensor Networks*, vol. 20, no. 2, pp. 1–21, 2024.

[30] A. Odena, C. Olah, and J. Shlens, "Conditional image synthesis with auxiliary classifier gans," in *International conference on machine learning*, pp. 2642–2651, PMLR, 2017.

[31] T. S. Rappaport, *Wireless communications: Principles and practice, 2/E*. Pearson Education India, 2010.

[32] H. S. Fahama, K. Ansari-Asl, Y. S. Kavian, and M. N. Soorki, "An experimental comparison of rssi-based indoor localization techniques using zigbee technology," *IEEE Access*, 2023.

[33] X. Zhu, W. Qu, X. Zhou, L. Zhao, Z. Ning, and T. Qiu, "Intelligent fingerprint-based localization scheme using csi images for internet of things," *IEEE Transactions on Network Science and Engineering*, vol. 9, no. 4, pp. 2378–2391, 2022.

[34] H. Yigit, "A weighting approach for knn classifier," in *2013 international conference on electronics, computer and computation (ICECCO)*, pp. 228–231, IEEE, 2013.

[35] C. R. Givens and R. M. Shortt, "A class of wasserstein metrics for probability distributions.," *Michigan Mathematical Journal*, vol. 31, no. 2, pp. 231–240, 1984.

[36] T. S. Rappaport, *Wireless communications: principles and practice*. Cambridge University Press, 2024.

[37] P. Series, "Propagation data and prediction methods for the planning of indoor radiocommunication systems and radio local area networks in the frequency range 900 mhz to 100 ghz," *Recommendation ITU-R*, pp. 1238–7, 2012.

[38] C. Liu, K. Wu, and T. He, "Sensor localization with ring overlapping based on comparison of received signal strength indicator," in *2004 IEEE International Conference on Mobile Ad-hoc and Sensor Systems (IEEE Cat. No.04EX975)*, pp. 516–518, 2004.

[39] P. Bahl and V. N. Padmanabhan, "Radar: An in-building rf-based user location and tracking system," in *Proceedings IEEE INFOCOM 2000. Conference on computer communications. Nineteenth annual joint conference of the IEEE computer and communications societies (Cat. No. 00CH37064)*, vol. 2, pp. 775–784, IEEE, 2000.

[40] M. Abbas, M. Elhamshary, H. Rizk, M. Torki, and M. Youssef, "Wideep: Wifi-based accurate and robust indoor localization system using deep learning," in *2019 IEEE International Conference on Pervasive Computing and Communications (PerCom*, pp. 1–10, IEEE, 2019.

[41] J. Wang, H. Jiang, J. Xiong, K. Jamieson, X. Chen, D. Fang, and B. Xie, "Lifs: Low human-effort, device-free localization with fine-grained subcarrier information," in *Proceedings of the 22nd Annual International Conference on Mobile Computing and Networking*, pp. 243–256, 2016.

[42] M. Youssef and A. Agrawala, "The horus wlan location determination system," in *Proceedings of the 3rd international conference on Mobile systems, applications, and services*, pp. 205–218, 2005.

[43] T. Gupta and H. Li, "Indoor mapping for smart cities — an affordable approach: Using kinect sensor and zed stereo camera," in *2017 International Conference on Indoor Positioning and Indoor Navigation (IPIN)*, pp. 1–8, 2017.

[44] C. X. Lu, S. Rosa, P. Zhao, B. Wang, C. Chen, J. A. Stankovic, N. Trigoni, and A. Markham, "See through smoke: robust indoor mapping with low-cost mmwave radar," in *Proceedings of the 18th International Conference on Mobile Systems, Applications, and Services*, pp. 14–27, 2020.